7th IFAC Symposium on Advances in Automotive Control
The International Federation of Automatic Control
September 4-7, 2013. Tokyo, Japan

Model based vertical dynamics estimation with Modelica and FMI

Michael Fleps-Dezasse, Jonathan Brembeck

Institute for System Dynamics and Control, Robotic and Mechatronic Center,
German Aerospace Center (DLR), Weßling, D-82234, Germany
(email: michael.fleps-dezasse@dlr.de, jonathan.brembeck@dlr.de)

Abstract: This paper analyses the performance of Modelica implemented state estimation algorithms for semi-active suspension control for the DLR ROboMObil (ROMO). In this approach the prediction model for the vertical dynamics state estimation and the tire contact force estimation is designed as a quarter vehicle model, which directly incorporates all relevant nonlinear parts. Based on this prediction model a square root unscented Kalman-filter (SR-UKF) is implemented, using the DLR Modelica Kalman-filter library and the Functional Mockup Interface (FMI). In a consecutive step this prediction model is extended by introducing an input port for road obstacle information, e. g. extracted from image data from ROMO 360 degree stereo surround view. The observer design and implementation on real-time hardware are performed in Modelica using the automated tool chain from the Modelica simulator to the Rapid Control Prototyping (RCP) hardware. Experimental results from a four post test-rig and simulations illustrate, that the estimation accuracy can be improved by the SR-UKF compared to an extended Kalman filter (EKF) based implementation.

Keywords: Kalman-filter, semi-active suspension, state estimation, Modelica, FMI

1 INTRODUCTION

The ROMO is an innovative robotic electric vehicle concept developed at the Robotics and Mechatronics Center of DLR. It is equipped with eight camera pairs meant for 360 degree stereo surround environment reconstruction and autonomous driving. The design of the ROboMObil is based on the "Wheel Robot" concept, see Brembeck et al. (2011a), which means that each of the four wheel units integrates the drivetrain, brakes, steering, spring and damper (see Figure 1). Therefore the wheel-sprung mass to body mass ratio raises to approx. $i_m = 1{:}\,3.5$, this is attributed to the transfer of the $16kW$ permanent-magnet synchronous motor (PMSM) into the wheel. The conflict between ride comfort and driving safety gets even more challenging to handle this way. A passive suspension system can only deal with this conflict with compromise in comfort aspects to ensure stability (Mitschke & Wallentowitz (2004)). Semi-active suspension systems mitigate this restriction by allowing a continuous and fast adaption of the damper force within their characteristic map. Furthermore they offer a reasonable compromise between energy consumption and performance compared to full active suspension systems (Williams (1994)). Because of this advantages, a lot of control strategies for semi-active dampers were discussed in literature over the last years. In Savaresi et al. (2010) an overview about control strategies for semi-active suspensions is presented and a performance evaluation scheme for this kind of suspension systems is introduced. Although there are control algorithms which do not require state feedback (Savaresi & Spelta (2009)) most advanced control strategies are based on adequate state feedback. However, the direct measurement of the required state quantities, especially the tire contact forces, is rather difficult to perform and state estimation is important for semi-active damper control. The drawbacks of measuring the tire deflection in motorcycle applications, e.g. by using optical distance sensors, are discussed in Delvecchio et al. (2011). In this paper they outline a linear Kalman-filter based estimation approach for a quarter vehicle model with special focus on the quality of the estimated tire deflection, which is in a first approximation directly related to the tire contact force. The authors evaluate the performance of these algorithms by means of experiments on a post test rig using varying sensor setups. In an earlier publication Delvecchio et al. (2010) analyze the quality of the estimated damper elongation and damper force in a similar suspension system including an electro-hydraulic (EH) damper. In Koch et al. (2010) and Koch et al. (2010a) further methods with focus on full state estimation for a quarter vehicle model are suggested. Koch et al. (2010) gives an overview of these methods by comparing a pure filter based approach, an EKF based approach and a third approach, employing three parallel linear Kalman-filters. Within the Kalman-filter setups, the nonlinear damper is modeled as a fictitious input as in Delvecchio et al. (2011). The performance of these approaches is analyzed in simulation and experiments on a quarter vehicle test bench, showing that the three parallel Kalman-filters provide a good compromise between computational effort and estimation accuracy.

In contrast to the above mentioned works, which mainly apply linear Kalman-filter techniques for state estimation, this paper outlines an EKF and a SR-UKF estimation approach implemented using the DLR Modelica Kalman-filter library (Brembeck et al. (2011)). Subsequently the SR-UKF algorithm is extended by introducing an additional input for road obstacle information to improve the observer accuracy during obstacle events (see section 4). The shape of

road obstacles like bumps and curbs can be extracted, for example from camera data (see Siegemund et al. (2010) and Siegemund et al. (2011)).

The paper is organized as follows. Section 2 presents the "Wheel Robot" and section 3 describes the nonlinear quarter vehicle model derived from the "Wheel Robot" of the ROboMObil. Section 4 presents the corresponding observer setups and section 5 the training of the observer setups by optimization techniques. Experimental results from a four post test rig and simulation results for obstacle crossing scenarios are given in section 6. This is followed by a short conclusion and description of future work in section 7.

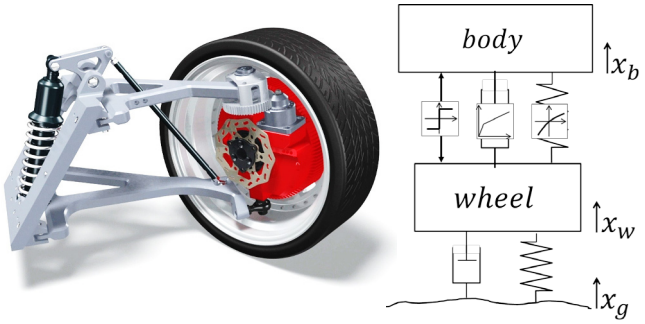

Figure 1: Left: the "Wheel Robot" concept, right: nonlinear two mass system

2 THE "WHEEL ROBOT"

The design of the "Wheel Robots" for the ROboMObil is described in detail in Brembeck et al. (2011a). As mentioned in section 1 the traction motors, brakes and steering system are integrated in the wheel itself, resulting in a large wheel-sprung mass. The suspension system is realized as a race-car oriented double wishbone layout. Its spring-damper unit is moved close to the subframe by use of a push rod-rocker kinematic (see Figure 1), which transmits the wheel motion to the spring-damper motion. The transmission ratio depends on the selected geometry of the suspension and can be designed independent of the control arms of the double wishbone suspension. It varies depending on the current suspension deflection (see Figure 2 right). Unlike the spring, which can be approximated by a linear stiffness function in our case, the speed-force characteristic of the damper is highly nonlinear (Figure 2 left).

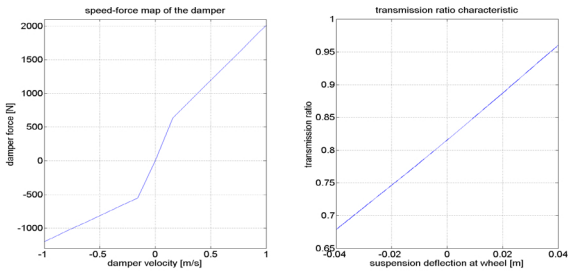

Figure 2: Left: Speed-force diagram of the nonlinear damper, right: suspension deflection-transmission ratio diagram

3 THE NONLINEAR QUARTER VEHICLE MODEL

Based on the "Wheel Robot" model, nonlinear quarter vehicle models with varying approximation depths are implemented in Modelica, depending on the purpose of the model. The tire stiffness and damping are assumed to be linear while modeling the "Wheel Robot" for observer design and simulation. The parameters of the "Wheel Robot" are given in Table 1.

Table 1. Parameters of the "Wheel Robot"

Parameter	Symbol	Value
Body mass	m_b	197.5 kg
Wheel mass	m_w	55.8 kg
Spring stiffness	k_b	20 kN/m
Tire stiffness	k_w	269 kN/m
Tire damping	d_w	650 Ns/m
Transmission ratio (K0)	i_{wb}	0.815

3.1 Multi-Body Model

For simulation studies a Modelica multi-body system (MBS) of the "Wheel Robot" including the double wishbone and the push rod-rocker kinematic with corresponding masses and inertias of all bodies is investigated. The model incorporates the above described spring-damper and tire characteristic supplemented by the friction force inside the damper. The damper is modeled by a speed-force map represented by characteristic points. In between these points, linear interpolation is used to approximate the speed-force behavior.

3.2 Two-Mass System

The simplified quarter vehicle model approximates the multi-body kinematic of the "Wheel Robot" by a two-mass system connected by the nonlinear spring-damper unit (Figure 1 right: structure). Therefore the masses of all suspension components and the vehicle body are merged into the two masses m_b and m_w of body and wheel. Next the approximated transmission ratio i_{wb} according to equation (1) is introduced.

$$i_{wb}(\boldsymbol{x}) = i_a + i_b * (x_w - x_b) \qquad (1)$$

This linear function with the parameters i_a and i_b constitutes a good approximation of the real transmission ratio connecting the spring-damper motion to the wheel and body motion. The tire and the spring-damper unit are modeled as described for the multi-body system. The same applies for the friction force inside the damper.

4 ESTIMATOR DESIGN

An introduction to Kalman-filter techniques and a detailed description of the square root unscented Kalman-filter can be found in Zarchan & Musoff (2005) and Simon (2006). A SR-UKF algorithm is better suited for highly nonlinear systems, because of its higher order linearization accuracy of mean and covariance compared to the EKF algorithm. Furthermore derivatives and Jacobians are not needed in a SR-UKF implementation, which supports the explicit consideration of

all relevant nonlinear parts like damper characteristic, friction and transmission ratio in the prediction model. Note that the damper is modeled as fictitious input to the prediction model in the EKF algorithm (Koch et al. (2010)). The detailed prediction model used inside the SR-UKF observer can further reduce the dependence of the state estimation on one specific sensor due to its more accurate system describtion.

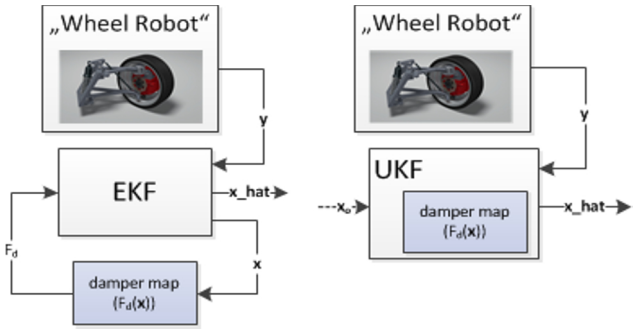

Figure 3: Kalman-filer structure: left – damper modeled as fictitious input, right – integrated damper

The estimators described below are implemented in Modelica simulator Dymola using the generic Kalman-filter library developed at DLR (Brembeck et al. (2011)). This library enables the fast implementation of nonlinear discrete observers with varying integration algorithms for the state prediction step like, *Trapezoidal* or *Runge-Kutta*. A Functional Mockup Unit (FMU) is used for the system and output evaluation inside the discrete observer algorithm. Therefore the continuous time Modelica model is first translated into a feasible FMU and subsequently the FMU is reimported to Modelica and is integrated as prediction model in the Kalman-filter setup. The observers analyzed in this paper use *Runge-Kutta 4* discretization with a sample period of $T_s = 4ms$ for state prediction. This choice was motivated by the sample period of the inertial measurement unit (IMU) mounted at the body, which also runs with a sample period of $4ms$. Figure 3 illustrates the structural difference between the layout of the SR-UKF and the EKF observer as explained in section 4.1, 4.2 and 4.3.

4.1 Quarter vehicle model with integrated nonlinear parts

Starting from the nonlinear two-mass system outlined in 3.2, the state representation of the "Wheel Robot", used for SR-UKF estimation, can be described as below (compare to Koch et al. (2010a) and Delvecchio et al. (2010)). The selected state vector $\boldsymbol{x}$ is given by:

$$\boldsymbol{x} = \begin{bmatrix} x_b & \dot{x}_b & x_w & \dot{x}_w & x_g \end{bmatrix} \quad (2).$$

The subscript b of the state variables indicates the position and velocity of the body, while the subscript w indicates the position and velocity of the wheel. The last state x_g represents the position of the ground. As mentioned in section 2, the "Wheel Robot" is equipped with an accelerometer measuring the acceleration $\ddot{z}_w$ of the upper control arm and a linear potentiometer measuring the damper deflection z_d. It is assumed that the acceleration error $\epsilon_{\ddot{z}_w}$ between the measured acceleration $\ddot{z}_w$ and the actual wheel acceleration (equation (3)) can be modeled as additional sensor noise.

$$\ddot{z}_w = \ddot{\bar{z}}_w + \epsilon_{\ddot{z}_w} \quad (3)$$

Additionally the acceleration $\ddot{\bar{z}}_b$ near the centre of gravity of the body is measured by the IMU. The acceleration of the body near the wheel is approximated from equation (4) by neglecting the roll and pitch dynamics $\boldsymbol{\alpha}_v$ and $\boldsymbol{\omega}_v$ of the vehicle body. In general this is not feasible and special care has to be taken to account for this approximation when defining the uncertainty of the body acceleration.

$$\Delta\ddot{\boldsymbol{z}}_b = \boldsymbol{\alpha}_v \times \boldsymbol{r}_{bw} + \boldsymbol{\omega}_v \times (\boldsymbol{\omega}_v \times \boldsymbol{r}_{bw})$$
$$\ddot{z}_b = \ddot{\bar{z}}_b + \Delta\ddot{z}_{b,z} \quad (4)$$

The vector of measurements $\boldsymbol{y}$ of the quarter vehicle model is shown below:

$$\boldsymbol{y} = [\ddot{z}_b \;\; \ddot{z}_w \;\; z_d] \quad (5).$$

In equation (6) the resulting state equations for the observer design are given. Unlike in Koch et al. (2010a) or in Delvecchio et al. (2010) the state equations are not linearized and the nonlinear parts like damper characteristic, friction and transmission ratio stay within the equations.

$$\dot{\boldsymbol{x}} = \begin{bmatrix} \dot{x}_b \\ \frac{1}{m_b}\left(F_s + F_d(\boldsymbol{x}) + F_f(\boldsymbol{x})\right) \\ \dot{x}_w \\ \frac{1}{m_w}\left(-F_s - F_d(\boldsymbol{x}) + F_{s,t} + F_{d,t} - F_f(\boldsymbol{x})\right) \\ -\beta v_v x_g \end{bmatrix} + \begin{bmatrix} w_{x_b} \\ w_{\dot{x}_b} \\ w_{x_w} \\ w_{\dot{x}_b} \\ w_{x_g} \end{bmatrix}$$

with

$$F_s = k_b i_{wb}(\boldsymbol{x})^2 (x_w - x_b)$$
$$F_{s,t} = k_w (x_g - x_w)$$
$$F_{d,t} = d_w (\dot{x}_g - \dot{x}_w) \quad (6)$$

The parameters m_b, m_w, k_b, k_w and d_w, are introduced in Table 1. All noises w_i of the state equations are assumed to be white, zero-mean Gaussian noise, describing the model uncertainties. The parameters β and v_v are part of the road model, which is included into the state equations to reduce the number of states. Based on the assumption that the power spectral density Φ_h of the road can be approximated by:

$$\Phi_h(\omega) = \frac{\alpha v_v}{\beta^2 {v_v}^2 + \omega^2} \quad (7),$$

with the angular frequency ω and the parameter α, the dynamics of the road profile can be formulated as (Mitschke & Wallentowitz (2004) and Koch et al. (2010a)):

$$\dot{x}_g(t) = -\beta v_v x_g(t) + w_{x_g}(t) \quad (8).$$

The parameter v_v represents the vehicle velocity and β is related to the road excitations. As mentioned in section 3.1, the damper is modeled by a speed-force map. The damper

force $F_d(\boldsymbol{x})$ included in the state equations, can be calculated using this map and the transmission ration by:

$$F_d(\boldsymbol{x}) = i_{wb}(\boldsymbol{x}) * F_{d,map}(i_{wb}(\boldsymbol{x}) * (\dot{x}_w - \dot{x}_b)) \quad (9).$$

The output force $F_{d,map}$ of the map depends on the damper velocity calculated from the wheel and body velocities scaled by the transmission ratio. The friction force F_f acting between body and wheel is calculated according to:

$$F_f(\boldsymbol{x}) = i_{wb}(\boldsymbol{x}) * F_{f,const} * tanh\left(\frac{\dot{x}_w - \dot{x}_b}{\epsilon_f}\right) \quad (10).$$

Here $F_{f,const}$ corresponds to a constant sliding friction and $tanh\big((\dot{x}_w - \dot{x}_b)/\epsilon_f\big)$ approximates the sign-function defining the direction of the friction force. The parameter ϵ_f is used to define transition behavior of the $tanh$-function.

The measurements are calculated from the current states by:

$$\boldsymbol{y} = \begin{bmatrix} \frac{1}{m_b}\Big(F_s + F_d(\boldsymbol{x}) + F_f(\boldsymbol{x})\Big) \\ \frac{1}{m_w}\Big(-F_s - F_d(\boldsymbol{x}) + F_{s,t} + F_{d,t} - F_f(\boldsymbol{x})\Big) \\ i_{wb}(\boldsymbol{x}) * (x_b - x_w) \end{bmatrix} + \begin{bmatrix} v_{\ddot{z}_b} \\ v_{\ddot{z}_w} \\ v_{z_d} \end{bmatrix} \quad (11).$$

The sensor noises $v_{\ddot{z}_b}$, $v_{\ddot{z}_w}$ and v_{z_d} are assumed to be white, zero-mean Gaussian noises.

4.2 Quarter vehicle model with separated nonlinear parts

The state and measurement equations presented in 4.1 used for SR-UKF estimation are adapted to fit the EKF scheme (Koch et al. (2010a)). Therefore the nonlinear damper characteristic is separated from the equations of the prediction model and regarded as a fictitious input to them (see Figure 3 left). Additionally the friction force is completely neglected. The remaining prediction model itself incorporates only a slight nonlinearity due to the transmission ratio. From these simplified state and measurement equations, the state and measurement Jacobians needed for the EKF prediction and update step can now be calculated analytically.

4.3 Quarter vehicle model with additional road obstacle input

Road obstacles can significantly deteriorate the ride comfort and driving safety of vehicles. This effect can be reduced by semi-active suspensions. The corresponding control algorithms require accurate state estimation, especially during the obstacle crossing period. If road obstacle information is provided to the observer, the estimation accuracy during obstacle events can be improved notably. Therefore an additional input $\dot{x}_o$ representing the current vertical obstacle velocity is introduced to the state equations and equation (8) representing the dynamics of the road is modified according to:

$$\dot{x}_g(t) = -\beta v_v x_g(t) + \dot{x}_o + w_{x_g}(t) \quad (12).$$

If no obstacle information is available, the input $\dot{x}_o$ is set to zero and the estimator is similar to 4.1. The signal $\dot{x}_o$ does not have to be very accurate to support the state estimation and improve the performance, see section 6.2. The experiments show that the estimation accuracy can be improved even if the shape of the obstacle is only known up to a scale factor as long as the phase shift of $\dot{x}_o$ with respect to the real obstacle event stays small.

5 ESTIMATOR TUNING

The parameters of the observers are set in two steps: first all known parameters like the model and sensor parameters are defined and second the remaining parameters are determined using optimization techniques. The known sensor variances are used to define the measurement covariance matrix R according to:

$$E\{\boldsymbol{v}_i \boldsymbol{v}_i^T\} = R = diag\big(\sigma_{\ddot{z}_b}^2\ \sigma_{\ddot{z}_w}^2\ \sigma_{z_d}^2\big) \quad (13),$$

with the standard deviation of the body acceleration $\sigma_{\ddot{z}_b}$ and the wheel acceleration $\sigma_{\ddot{z}_w}$, both increased to include the approximations described in section 4.1 and the standard deviation of the damper deflection σ_{z_d}, set to: $\sigma_{\ddot{x}_b} = 0.3\frac{m}{s^2}$, $\sigma_{\ddot{x}_w} = 0.2\frac{m}{s^2}$ and $\sigma_{z_d} = 0.001m$.

The optimization is done in the Modelica simulator Dymola using the optimization library version 2.1 developed at DLR (see Pfeiffer (2012)). The library enables nonlinear optimization, like sequential quadratic programming (SQP) or genetic algorithms with boundary constraints. The parameter vector $\boldsymbol{\Theta}$ includes the diagonal entries of the prediction covariance matrix $\boldsymbol{Q}$. From $\boldsymbol{Q}$ the initial state covariance matrix $\boldsymbol{P}_{ini}$ is calculated by: $\boldsymbol{P}_{ini} = \alpha_P * \boldsymbol{Q}$, with $\alpha_P = 10$ determined by a previous optimization run using the initial vales for the parameters $\boldsymbol{\Theta}$.

The overall cost function J of the optimization at hand is defined as:

$$J = \sum_{i=1}^{m} \frac{1}{\omega_i} J_i \quad (14).$$

It incorporates four parts ($m = 4$): part one to three compare the simulated signals (body velocity, wheel velocity and tire force) of the simplified quarter vehicle model (section 3.2) subject to stochastic road excitations to the corresponding estimated signals and part four compares the measured tire force on the four post test rig excited by a sine sweep to the estimated tire force. The weights ω_i are set in such a way, that the measured tire force is prioritized. In the absence of real state measurements, the simulation parts are added to the optimization setup to achieve a balanced optimization result with focus on full state estimation. The cost function J_i is calculated from:

$$J_i = \frac{\sum_{n=1}^{N}(y_{i,n} - \hat{y}_{i,n})^2}{\sum_{n=1}^{N}(y_{i,n} - y_{mean})^2} \quad (15).$$

This definition represents the relative Mean Square Error (MSE) of the estimated signal $\hat{y}_{i,n}$ compared to the simulated or measured signal $y_{i,n}$ where y_{mean} represents the mean value of $y_{i,n}$. The optimization problem is stated in (16).

$$\text{argmin}_{\boldsymbol{\theta}}(J) \qquad subject\ to \begin{matrix} \boldsymbol{\theta} < \boldsymbol{\theta}_{max} \\ \boldsymbol{\theta} > \boldsymbol{\theta}_{min} \end{matrix} \qquad (16)$$

Table 2 illustrates the difference between the estimation accuracy with the initial parameters and the optimized parameters by means of the coefficient of determination $R_i^2 = 1 - J_i$ calculated from the cost function J_i. A R_i^2 value of one indicates a perfect fit between estimated and measured signal, while a R_i^2 value of zero indicates an estimation error as large as the signal variance.

Table 2. Optimization results compared to initial results

Estimator type	EKF_{ini}	$SR\text{-}UKF_{ini}$	EKF_{opt}	$SR\text{-}UKF_{opt}$
$R^2_{\dot{x}_b}$	0.576	0.693	0.741	0.776
$R^2_{\dot{x}_w}$	0.724	0.808	0.810	0.851
$R^2_{F_{z,sim}}$	0.939	0.965	0.951	0.986
$R^2_{F_{z,m}}$	0.904	0.908	0.914	0.904

The parameterization of the initial observers is the same. As can be seen, the overall state estimation of the SR-UKF is better, while the EKF has a strong focus on the contact force.

6 EXPERIMENTAL AND SIMULATION RESULTS

The evaluation of experimental and simulation results is carried out as described in section 5 by means of comparing the coefficient of determination R_i^2. A dSpace simulator is used as RCP. The detailed semi-automated tool chain from the Kalman-filter library to RCP will be discussed in a later publication.

6.1 Experimental Results

Results from full vehicle experiments on the post test rig are given in Table 3 and Figure 5. Figure 4 illustrates the experimental setup. As mention in section 5 the velocities of body and wheel were not measured and thus the evaluation is performed comparing only the contact forces.

Figure 4: ROMO on the four post test rig

Three different excitations are illustrated: a sine sweep, a test drive on the race track "Nordschleife" and a test drive on a rough road at "Oschersleben". The estimation performance when looking at the tire contact force of the observers is almost the same for the sine sweep. In contrast to the good estimation results during the sine sweep excitation, the estimation performance of both observers deteriorates during the other excitations. This indicates that the assumption concerning the roll and pitch dynamics made in section 4.1 is no longer valid and the roll and pitch dynamics of the body have to be considered for better estimation results (see Table 3 and Figure 5). Especially the SR-UKF observer, which integrates the damper, suffers from the rather bad body acceleration measurement due to its stronger linkage between body and wheel motion inside its state equations.

Table 3. Performance of EKF and SR-UKF on a four post test rig

Estimator type	Excitation	EKF	SR-UKF
$R^2_{F_z}$	Sine Sweep	0.914	0.904
$R^2_{F_z}$	Nordschleife	0.512	-0.06
$R^2_{F_z}$	Oschersleben	0.281	0.190

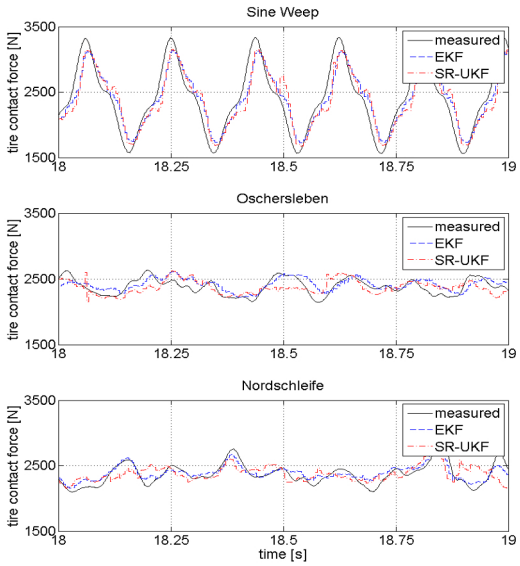

Figure 5: Comparison of the contact force estimation on the four post test rig: above "Sine Sweep", middle "Oschersleben" and below "Nordschleife"

6.2 Simulation Results

The robustness and performance improvement by including obstacle information in the prediction model is analyzed in simulation using the multi-body quarter vehicle model (section 3.1). Therefore the extended $SR\text{-}UKF_{xo}$ observer (section 4.3) is compared to the SR-UKF observer (section 4.1). The results are shown in Table 4 and Figure 6. Three setups with respect to the quality of the provided obstacle information are analyzed. Setup 1 assumes perfect knowledge of the obstacle shape and occurrence, in setup 2 the obstacle shape is only known up to a scale error of 0.5 and in setup 3 additionally to the scale error, the input signal $\dot{x}_o$ is delayed by $50ms$. As can be seen in Table 4, the additional obstacle information improves the estimation accuracy, especially when the overall state estimation is considered. By comparing the three setups described above it can be seen,

that the estimation accuracy of the body motion is more sensitive to the quality of the provided obstacle information then the wheel motion or the contact force estimation. Further it is obvious, that an accurate temporal alignment of the obstacle information with respect to the vehicle is more crucial than the accurate shape of the obstacle. This is notable when looking at the large decrease of the accuracy in setup 3 (scale error and delay) compared to the rather small decrease in setup 2 (scale error only).

Table 4. Estimation performance with obstacle information and without obstacle information

Estimator type	SR-UKF	SR-UKF$_{xo}$ setup 1	SR-UKF$_{xo}$ setup 2	SR-UKF$_{xo}$ setup 3
$R^2_{\dot{x}_b}$	0.695	0.826	0.809	0.717
$R^2_{\dot{x}_w}$	0.772	0.780	0.785	0.711
$R^2_{F_z}$	0.777	0.822	0.827	0.801

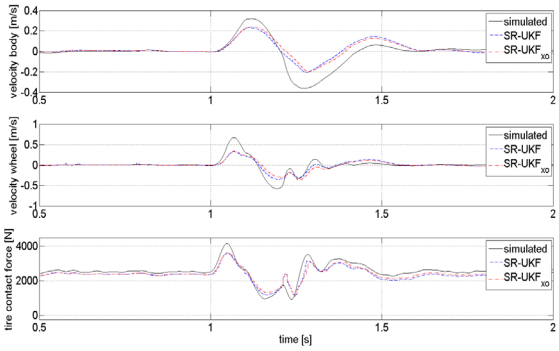

Figure 6: Comparison of the estimation during obstacle event (SR-UKF$_{xo}$ setup 3)

7 CONCLUSION

In this paper an SR-UKF observer for a quarter vehicle was developed and in a subsequent step this observer was extended with obstacle information. The performance of the observer was analyzed in simulation and experiments on a four post test rig. Future work on quarter vehicle state estimation will focus on the extension of the suspension system by a semi-active damper and on the consideration of roll and pitch dynamics of the vehicle body. Further the cameras of ROMO will be used to provide obstacle information.

8 ACKNOWLEDGEMENTS

The authors would like to thank Dr. Bals for his support and Uwe Bleck for his expertise in questions of applied vehicle dynamics. A special thank of the authors goes to Dr. Andreas Pfeiffer supporting this research with its expertise in Modelica implementation and automatisation of the DLR Kalman Filter library and his great support in application questions of the DLR Optimization library.

REFERENCES

Brembeck, J., Ho, L. M., Schaub, A., Satzger, C. & Hirzinger, P. G. (2011a), Romo - the robotic electric vehicle, *in* 'International Association for Vehicle System Dynamics (IAVSD)'.

Brembeck, J., Otter, M. & Zimmer, D. (2011), Nonlinear observers based on the functional mockup interface with application to electric vehicles, *in* 'Modelica 2011 Conference'.

Delvecchio, D., Spelta, C., Perico, G. & Savaresi, S. (2010), Accelerometer-based estimation of the elongation speed in a motorcycle suspension via kalman-filter techniques, *in* 'Decision and Control (CDC), 2010 49th IEEE Conference on', pp. 5566 –5571.

Delvecchio, D., Spelta, C. & Savaresi, S. (2011), Estimation of the tire vertical deflection in a motorcycle suspension via kalman-filtering techniques, *in* 'Control Applications (CCA), 2011 IEEE International Conference on', pp. 532 –537.

Koch, G., Kloiber, T. & Lohmann, B. (2010), Nonlinear and filter based estimation for vehicle suspension control, *in* 'Proc. 49th IEEE Conf. Decision and Control (CDC)', pp. 5592–5597.

Koch, G., Kloiber, T., Pellegrini, E. & Lohmann, B. (2010a), A nonlinear estimator concept for active vehicle suspension control, *in* 'Proc. American Control Conf. (ACC)', pp. 4576–4581.

Mitschke, M. & Wallentowitz, H. (2004), *Dynamik der Kraftfahrzeuge*, Berlin: Springer.

Pfeiffer, A. (2012), Optimization library for interactive multi-criteria optimization tasks, *in* 'Modelica 2012 Conference'.

Savaresi, S., Poussot-Vassal, C., Spelta, C., Sename, O. & Dugard, L. (2010), *Semi-Active Suspension Control Design for Vehicles*, Elsevier Science.

Savaresi, S. & Spelta, C. (2009), 'A single-sensor control strategy for semi-active suspensions', *Control Systems Technology, IEEE Transactions on*, 143 –152.

Siegemund, J., Franke, U. & Förstner, W. (2011), A temporal filter approach for detection and reconstruction of curbs and road surfaces based on conditional random fields, *in* 'Intelligent Vehicles Symposium (IV), 2011 IEEE', pp. 637 – 642.

Siegemund, J., Pfeiffer, D., Franke, U. & Förstner, W. (2010), Curb reconstruction using conditional random fields, *in* 'Intelligent Vehicles Symposium (IV), 2010 IEEE', pp. 203 –210.

Simon, D. (2006), *Optimal State Estimation: Kalman, H Infinity, and Nonlinear Approaches*, Wiley.

Williams, R. (1994), 'Electronically controlled automotive suspensions', *Computing Control Engineering Journal*

Zarchan, P. & Musoff, P. (2005), *Fundamentals Of Kalman Filtering: A Practical Approach*, number Bd. 208 *in* 'Progress in Astronautics and Aeronautics Series', Amer Inst of Aeronautics.